*Proc. Natl. Acad. Sci. USA*
Vol. 93, pp. 10647–10652, October 1996
Biochemistry

# Structure of the replication terminus–terminator protein complex as probed by affinity cleavage

**(termination of replication/protein–DNA interaction)**

KARNIRE S. PAI*, DIRKSEN E. BUSSIERE*, FENGGANG WANG†, STEPHEN W. WHITE*, AND DEEPAK BASTIA*‡

*Department of Microbiology, Duke University Medical Center Durham, NC 27710; and †Department of Microbiology, University of North Carolina, Chapel Hill, NC 27599

*Communicated by Clyde A. Hutchison III, University of North Carolina, Chapel Hill, NC, July 29, 1996 (received for review, June 5, 1996)*

**ABSTRACT** **The replication terminator protein (RTP) of *Bacillus subtilis* is a homodimer that binds to each replication terminus and impedes replication fork movement in only one orientation with respect to the replication origin. The three-dimensional structure of the RTP–DNA complex needs to be determined to understand how structurally symmetrical dimers of RTP generate functional asymmetry. The functional unit of each replication terminus of *Bacillus subtilis* consists of four turns of DNA complexed with two interacting dimers of RTP. Although the crystal structure of the RTP apoprotein dimer has been determined at 2.6-Å resolution, the functional unit of the terminus is probably too large and too flexible to lend itself to cocrystallization. We have therefore used an alternative strategy to delineate the three dimensional structure of the RTP–DNA complex by converting the protein into a site-directed chemical nuclease. From the pattern of base-specific cleavage of the terminus DNA by the chemical nuclease, we have mapped the amino acid to base contacts. Using these contacts as distance constraints, with the crystal structure of RTP, we have constructed a model of the DNA–protein complex. The biological implications of the model have been discussed.**

Replication of the chromosome of *Bacillis subtilis* is initiated at an unique origin, and under normal conditions the forks progress bidirectionally until converging at six sequence-specific replication termini that are located approximately 180° from the origin (1–3). The terminus IR1 (Ter1) appears to be the most frequently used site for replication fork arrest *in vivo* (4). Each terminus arrests replication forks *in vivo* and *in vitro* in only one orientation with respect to the replication origin (4–6). The replication terminator protein (RTP) specifically binds as two interacting dimers to each terminus (7–9). RTP is functional *in vivo* (10) and *in vitro* (5, 6, 11) in the surrogate Gram-negative *Escherichia coli* system and arrests the replicative helicases DnaB and PriA of *E. coli* in a polar mode (5, 6, 9, 11).

RTP is a homodimeric protein with subunit molecular mass of 14.5 kDa (12, 13). The crystal structure of RTP has been determined at 2.6-Å resolution and the structure reveals a disordered N-terminal arm, four α-helices, and three antiparallel β-strands. The β2- and β3-strands are connected by an extended loop and the two α4-helices of the two monomers form an antiparallel coiled-coil dimerization domain. The overall structure is a winged helix with the β2- and β3-strands and the connecting loop of the two monomers forming the two wings and the α1-, α2-, and α3-helices forming the prototypical helices of the winged helix (Fig. 1 and ref.14). Two interacting dimers of RTP, bound to the overlapping core and the auxiliary sites, are necessary to impede replication forks (9). We have shown that the β3-strands and the tip of the extended loop that connects β2 with β3 are both necessary for dimer–dimer interaction (9). Mutational analyses and biochemical studies have shown that the N-terminal arm, the β2-strand, and the α3-helix of RTP are involved in DNA binding (15).

Although the structure of the RTP dimer is symmetrical (14), the protein impedes fork movement in an asymmetric mode (5–7, 9). It is reasonable to suspect that the interaction of the protein with DNA might provide the structural basis of the functional polarity. To understand the mechanistic details of replication fork arrest, it will be necessary to determine the structure of the RTP–DNA complex. The minimum functional unit of the replication terminus of *B. subtilis* consists of four turns of DNA and two interacting dimers of RTP, a structure that is perhaps too large and too flexible to lend itself to cocrystallization. We have therefore resorted to an alternative approach to derive a model of the three-dimensional structure of the DNA–protein complex. The approach consisted of the conversion of RTP into a site-directed chemical nuclease and the use of the nuclease to cleave the DNA at the contact points (16–19). Using the contact points as distance constraints, we have constructed a three-dimensional model of the RTP–terminus DNA complex. The model reveals that the contacts made by the RTP dimers with the core and the auxiliary sites forming the terminus are indeed dissimilar, thus providing a basis for the predicted structural asymmetry. The model also reveals the surface of the protein that is likely to make contacts with the approaching helicase.

## MATERIALS AND METHODS

**Oligonucleotides, DNAs, and Plasmids.** The two strands of the core and IR1 DNAs were synthesized, end-labeled, and annealed so that only one 5′ end was labeled at a time. In some cases, the synthetic DNAs were cloned at the multilinker sites of pUC18/19 vector DNAs and excised and end-labeled in such a way as to add spacer sequences at either end. The labeled DNAs were used to form complexes with the ethylenediaminetetraacetic acid 2-aminoethyl 2-pyridyl disulfide (EPD)-conjugated wild-type and mutant RTPs.

**Site-Directed Mutagenesis.** Site-directed mutagenesis was performed as described (20) to substitute Cys residues at various locations in the regions of RTP known to be involved in DNA binding (15). The following mutations were isolated: R16C located in the α1 helix; E56C, R59C, and E63C located in the α3 helix; and K74C located in the β2-strand of RTP (see Fig. 1).

**Derivatization of the Proteins with EPD and Affinity Cleavage.** The wild-type and the mutant forms of RTP were purified, as described (6). The wild-type protein, which has a single Cys at the position 110 (12), and the mutant forms having the natural and the second Cys substituted at the indicated sites,

The publication costs of this article were defrayed in part by page charge payment. This article must therefore be hereby marked "*advertisement*" in accordance with 18 U.S.C. §1734 solely to indicate this fact.

Abbreviations: RTP, replication terminator protein; EPD, ethylenediaminetetraacetic acid 2-pyridyl,2-aminoethyl disulfide.

‡To whom reprint requests should be addressed.

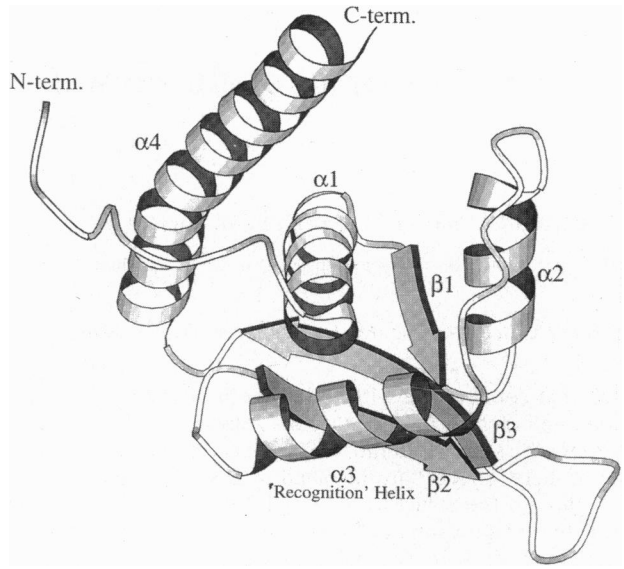


FIG. 1. Ribbon diagram of RTP based on the crystal structure. Note the four α-helices, three β-strands, an unstructured N-terminal region, and an extended loop connecting β2 to β3. The α3-helix was postulated to contact the major groove and the β2-strand and the loop connecting β2 to β3, to contact the minor groove. The dimerization domain consists of two coiled-coil α4-helices belonging to the two monomers forming the dimer. The dimer–dimer interaction domain is located on the β3-strand (9, 14).

were derivatized with EPD, as described (17, 18). Wild-type and Cys-substituted RTPs (100–200 μg) were treated with 3 mM EPD in 100 mM Tris·HCl, pH 7.3/1 M NaCl at 4°C for 36 h. Unreacted EPD was removed by dialysis against 25 mM Tris·HCl, pH 7.3/50 mM NaCl for 2 h at 4°C. The extent of derivatization was measured using Ellman's reagent, as described (16, 17). The derivatized RTPs (100–200 ng) in 100 μl of 10 mM Mops·NaOH, pH 7.3/200 mM NaCl/BSA (50 μg/ml)/1 mM ascorbic acid were incubated at 23°C for 3 h. The DNA was ethanol-precipitated in the presence of 5 μg of tRNA and analyzed in 15–20% polyacrylamide/8 M urea gels.

**Computational Modeling of the RTP–DNA Complex.** When cleavage of DNA is induced by a Fe-EDTA-conjugated binding protein, cleavage occurs at the C1′ and/or C4′ bonds of the deoxyribose moieties within a distance of 3–4 Å from the location of the hydroxyradical generator, the Fe atom (16, 18, 21). The chelated Fe is located at a distance of 14 Å from the α-carbon atom of the conjugated Cys. Therefore, cleavage occurs at a net distance of 14 ± 3–4 Å from the α-carbon of the Cys residues. This consideration allowed a distance constraint to be assigned to the locations of the Cys conjugates on RTP and the corresponding cleavage sites on DNA. The cleavage data were converted to distance constraints for use with the X-PLOR program package (22). The distance constraints were converted to an energy term for the molecular force field by being modeled as NOE (nuclear Overhauser effect) distance restraints, which are normally assigned to interproton distances during structural analysis by NMR. It should be noted that no direct energetic relationship between the Fe-EDTA and the contacted bases are implied in the procedure; rather, the NOE term appears to be a convenient way to translate the affinity cleavage data into distance constraints used to build the model. The model consisted of two dimers of RTP positioned 15 Å from the axis of the terminus DNA (modeled as a linear duplex of B form) with the dyad axes positioned parallel to the center of each of the two subsites (i.e., core and auxiliary sites). The most successful energy minimization simulation involved defining each secondary feature of the protein and each planar sugar moiety and base of the DNA as a rigid body that was allowed six degrees of freedom—three translational and three rotational. The relative positions of the atoms within a rigid body were not allowed to change independently. A second approach used Powell energy minimization to gradually and reproducibly reduce the overall energy of the simulated structure. The energy terms included van der Waals interactions, electrostatic interactions, hydrogen bonding, and bond energies. To maintain the integrity of the planar bases, a planarity term was introduced to prevent nucleotide base buckling.

## RESULTS

**Conversion of RTP into a Chemical Nuclease and Cleavage of the Residues of the Core Site.** Previous work has shown that the N-terminal arm, the β2-strand, and the α3-helix of RTP participate in DNA binding (15). We introduced Cys residues at various locations of the three regions of RTP and derivatized the Cys residues with EPD using the exchange reaction shown in Fig. 2*A* (16–19, 21). If the derivatized residue either contacts DNA or is located within 14 Å of the DNA, then in the presence of ascorbate, localized cleavage of the DNA is induced by generation of hydroxyradicals. The pattern of cleavage depends on whether the Fe moiety is positioned on the minor or the major groove of the DNA. Minor groove location causes cleavage at the C1′ and C4′ residues of the sugar at the minor groove in such a way that the cleavage sites are displaced toward the 3′ end. Major groove location causes the diffusion of the hydroxyradicals to the two adjacent minor grooves and the cleavage pattern is shifted to the 5′ ends (Fig. 1*B* and ref. 21). This is because the C1′ and the C4′ bonds are available for cleavage only in the minor grooves. The right-handed nature of the DNA double helix also shapes the cleavage pattern (21). The expected cleavage pattern (Fig. 2*B*)

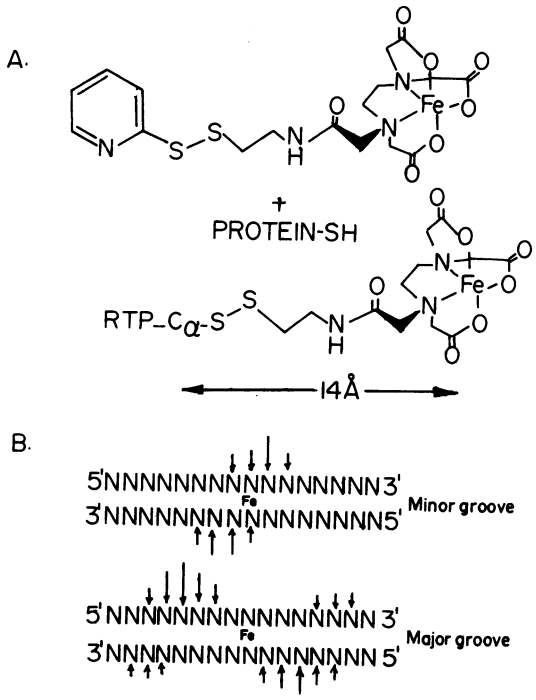


FIG. 2. Conversion of RTP into a chemical nuclease. (*A*) Scheme of the exchange reaction that couples a solvent accessible Cys group in RTP with EPD. (*B*) Cleavage patterns generated when the Fe moiety (indicated at the center of the sequence) contacts the minor and the major grooves of DNA. The cleavage pattern is caused by the cleavage of the C1′ and C4′ bonds that are exposed in the minor grooves and due the right-handed nature of the DNA double helix (see ref. 21).

can change if protein–DNA contacts block one or more of the cleavage sites.

Gel mobility shift experiments were performed to determine if EPD conjugation at the appropriate sites of RTP caused abolition of DNA binding. With the exception of the residue 59, where EPD conjugation did not reduce the strength of DNA binding, Cys substitution followed by EPD conjugation caused detectable reduction but not total abolition of DNA binding (data not shown).

We first wished to determine the amino acid–DNA base contacts of a single dimer of RTP bound to an isolated core site and subsequently to compare and contrast the pattern with that generated by the binding of two interacting dimers to the functional IR1 (Ter1) terminus. The top and the bottom strands of core site DNA was 5′-end-labeled and complexed with wild-type RTP that was derivatized at the single naturally occurring Cys present at the position 110 of the α4-helix (Fig. 1). We also complexed the DNA with RTP derivatized at the site R16C of the α1-helix, K74C of the β2-strand, and the residues R59C and E63C of the α3 recognition helix. We substituted a Cys at the position Q72 of the β2-strand but discovered that the mutant form of the protein was insoluble. We also derivatized the N-terminal arm at the sites 4 and 8 but found that these derivatives did not cleave DNA. The wild-type RTP that was derivatized at the single Cys located at position 110 in the α4-helix that is known not to contact DNA (15) did not cause DNA cleavage thus serving as a negative control (see Figs. 5 and 6).

The cleavage patterns of the isolated core sequence by the protein, derivatized at the positions 16, 59, 63, and 74, are shown in Fig. 3 *A* and *B*. The G>A cleavage products of the same end-labeled DNAs were used as a ladder of molecular size markers to assign unambiguously the sites of cleavage. The R16C protein derivative cleaved the core site at the coordinate 28 on both strands of the DNA. The E63C protein derivative also cleaved the core sequence at the same location. This observation is understandable in the light of the fact that R16 is located only 9 Å away from the residue E63 although the two residues are located in two different α-helices. In contrast with R16C and E63C, the R59C derivative cleaved both strands of the core DNA at several locations in two clusters that probably correspond to the contacts of the two α3-helices of the dimeric protein. The cleavage patterns are summarized in Fig. 4. We also prepared Fe-EDTA conjugated at E56C and complexed it with the core sequence but failed to detect, in three experiments, any cleavage of the DNA. However, crosslinking studies using azidophenacyl bromide introduced at E56C, showed crosslinkage to DNA when irradiated with ultraviolet radiation (data not presented), suggesting thereby that E56C indeed contacted the core site probably at a location equivalent to that observed in IR1 DNA.

The K74C derivative cleaved the DNA also in two clusters with the cleavage sites displaced toward the 3′ ends of the DNA. The pattern of cleavage suggests that the Fe moiety at K74C of RTP is positioned in the minor groove of the DNA.

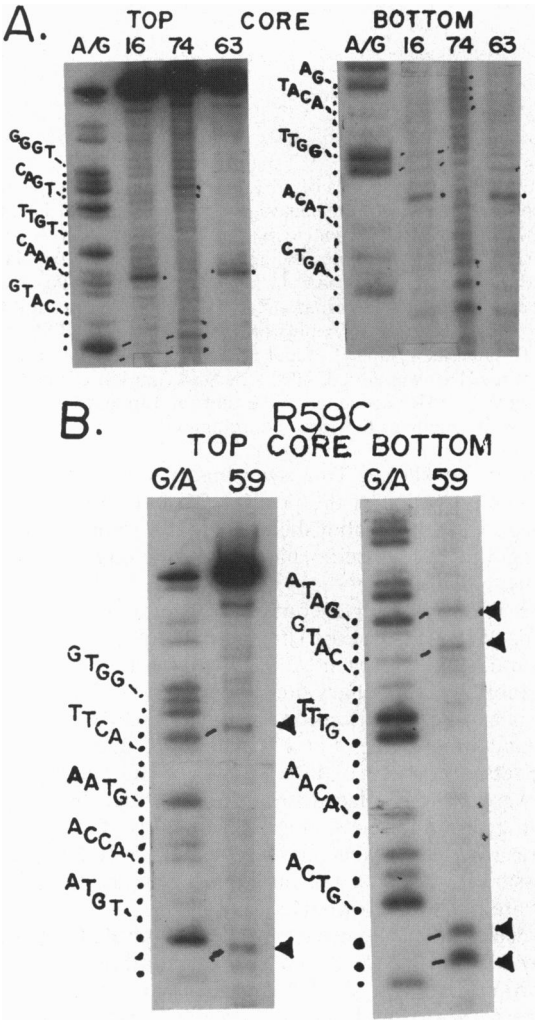


FIG. 3. Autoradiograms of 15% polyacrylamide/urea denaturing gels showing the cleavage patterns of core DNA by various Fe-EDTA derivatives of RTP. (*A*) Autoradiograms showing the cleavage patterns of the top and the bottom strands of core DNA caused by R16C, K74C, and E63C derivatives of RTP. A/G, G>A sequencing ladder; the DNA sequence of the core is shown on the left; 16, 74, and 63 denote the cleavage patterns of the RTP–EPD derivatives. (*B*) Cleavage of core DNA by R59C. A/G denotes G> A DNA sequence ladder; 59 designates the cleavage patterns of the top and bottom strands by derivatized R59C RTP. Arrowheads indicate the major cleavage sites. Note that control experiments were also performed using wild-type RTP that was conjugated with EPD at the Cys located at the position 110 (α4-helix; Fig. 1). No cleavage was detected when the wild-type EPD conjugate was used in the reaction mixture (data not shown; however, see Figs. 5 and 6).

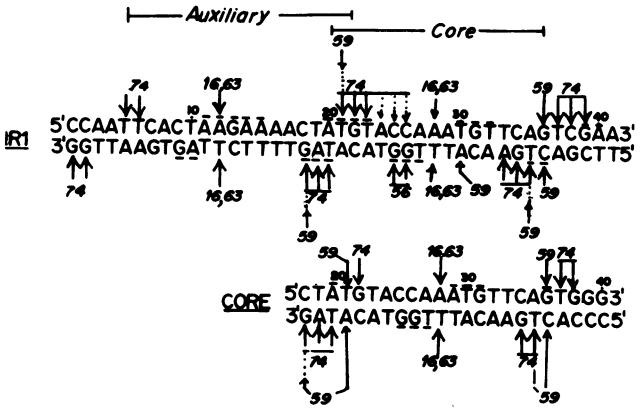


FIG. 4. Summary of the interactions of the various EPD derivatives of RTP with the the IR1 (*Upper* sequence) and the isolated core sequence (free from the adjacent auxiliary site; *Lower* sequence). Dotted lines immediately over or under a base indicates protection from hydroxyradicals. The smaller nonitallicized numbers mark the DNA sequence coordinates. The larger italicized numbers with arrows show the major cleavage sites by RTP derivatized at the amino acids 16, 56, 59, 63, and 74. Discontinuous arrows indicate the minor cleavage sites. IR1 is the most frequently used terminus also known as Ter1. Core indicates an isolated core sequence lacking the auxiliary site. *A, B, C,* and *D* designate the monomers that are arranged as two interacting dimers with the arrangement A–B and C–D with the former dimer contacting the auxiliary and the latter contacting the core site. The monomers B and D are interacting at their β3-strands to promote dimer–dimer interaction.

It should be noted that K74C cleaved at the first three residues of the isolated core sequence (Fig. 4 *Lower*) that were contributed by the polylinker of the vector. Therefore, the K74C derivative cleaved DNA just outside of the real core sequence (thus suggesting that β2-strand contacts the DNA in the minor groove in a nonsequence-specific mode; Fig. 3*A*). To ensure that the cleavage was generated by the EPD-derivatized RTP, a series of control experiments were performed (Figs. 4 and 5) that showed that only the derivatized Cys residues and not the underivatized ones and not EPD by itself or the wild-type RTP conjugated at the natural Cys located at cordinate 110, yielded detectable specific cleavage of the DNA.

**Mapping the Cleavage Sites on the IR1 (Ter1) DNA.** The IR1 (Ter1) is one of the most frequently used terminus of *B. subtilis* (3, 12) and consists of overlapping core and auxiliary sites that bind to two interacting RTP dimers (6, 7, 9). We used the EPD conjugates of the derivatives R16C, E56C, R59C, E63C, and K74C to cleave 5′-end-labeled IR1 DNA. The cleavage products were resolved in a DNA sequencing gel with the appropriate G + A sequence ladder that was used to identify the sites of cleavage. The autoradiograms of the cleavage induced by E56C (Fig. 5) and R16C are shown (Fig. 6). R16C induced major cleavages on both strands of the DNA at the coordinate 12 and 28 of the IR1 sequence. Surrounding the major cleavage sites, several minor cleavage sites were also visible over the back ground noise of nonspecific cleavage (Figs. 5 and 6). Cleavage of the bottom but not that of the top strand was detectable in the presence of the E56C derivative. The bottom strand showed a major cleavage at the residue 25 and a minor one at residue 26 (Fig. 6). Thus, E56C seems to contact only the bottom strand of the core but not that of the auxiliary site, thereby contributing to the asymmetry of the DNA–protein complex. Does E56C contact base-specific at the G25 residue or does the contact occur on the sugar phosphate backbone? To answer this question, we introduced a G → T mutation at the position 25 and observed that the cleavage was either abolished or greatly reduced, thus confirming the base-specific nature of the contact (data not shown).

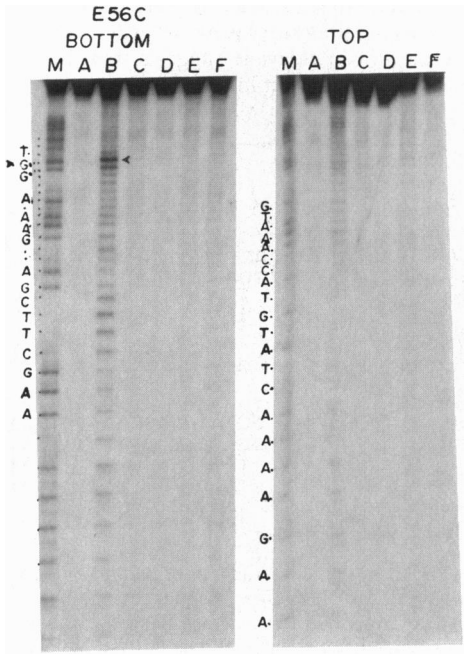


FIG. 5. Autoradiograms of 15% polyacrylamide/urea denaturing gels showing the cleavage patterns of IR1 DNA by derivatized RTPs. Cleavage pattern of the top and bottom strands by E56C. Lanes: M, G>A sequence ladder; A, labeled DNA plus ascorbate; B, labeled DNA plus E56C derivative plus ascorbate; C, wild-type RTP-EPD derivative plus labeled DNA + ascorbate; labeled DNA plus R56C-EPD derivative; E, labeled DNA plus underivatized E56C RTP plus ascorbate; F, same as in lane B but with a 50-fold excess of competing unlabeled DNA. The only detectable cleavages are a major site (arrowhead) and an adjacent minor site (dot) in lane B, bottom strand.

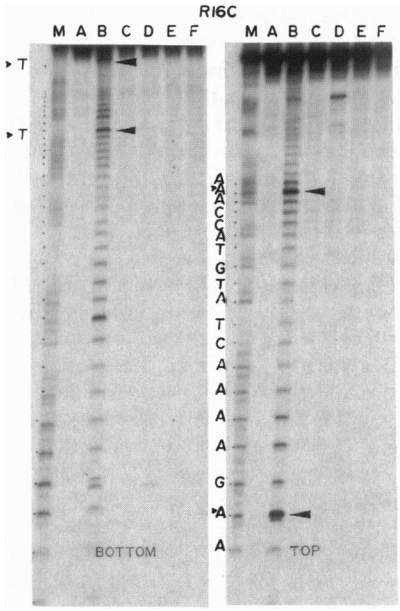


FIG. 6. Autoradiograms of 15% polyacrylamide/urea sequencing gels showing the pattern of cleavage of both strands of labeled IR1 DNA by R16C-EPD derivative. Lanes: M, G + A DNA sequence ladder; A, labeled DNA plus ascorbate; B, labeled DNA plus R16C-EPD derivative plus ascorbate; C, labeled DNA plus wild-type RTP-EPD derivative plus ascorbate; D, labeled DNA plus R16C-EPD derivative; E, labeled DNA plus underivatized R16C RTP + ascorbate; F, same as in lane B except that a 50-fold excess of unlabeled competitor DNA was added. The arrowheads mark the major cleavage sites within the IR1 sequence. Note that the top and bottom strands are cleaved exactly at the same coordinates.

The R59C derivative contacted several residues on both strands of IR1, at the core site and in the region shared by the core and the auxiliary sites (Fig. 4). No other contacts were detectable in the auxiliary site. The contacts of R59C with IR1, thus, is another contribution to the asymmetry of the DNA–protein complex (Figs. 4 and 7). The K74C derivatives showed three sets of contacts on both strands of IR1 and the cleavage sites were again displaced toward the 3′ side, thus suggesting minor groove contacts (Figs. 3*A* and 4). Comparing and contrasting the contacts on the core and the IR1 sequences, it is possible to visualize the outlines of how the two dimers of RTP are positioned on IR1.

**Hydroxyradical Footprints of Wild-Type RTP on the Core and the IR1 Sequences.** To derive a general picture as to how the protein contacts the DNA, under our experimental conditions, we performed hydroxyradical footprinting of wild-type RTP on the core and the IR1 sequences. The data are not shown but the results are summarized in Fig. 4 (lines over and under the bases of both strands of the sequences). The site-directed contacts derived from the EPD derivatives, as expected, overlapped some of the nucleotides protected by RTP, as revealed by the hydroxyradical footprints. One objective of the hydroxyradical footprinting was to determine whether the two interacting β3-strands invoved in dimer–dimer interaction contacted residues 20 and 21 of the IR1 sequence. There was indeed protection of the region of residues 20–23 of the top and residues 18–20 of the bottom strands of IR1 (Fig. 4).

**Computational Modeling of the RTP–IR1 Complex.** Existing data showed that cleavage of DNA occurred within 14 ±

3 Å of the α-carbon of the substituted Cys moiety. The computational modeling took into consideration the following information about the RTP–DNA complex. First, the complex contains approximately four turns of DNA and two interacting dimers of RTP (6, 7, 9, 23). There was minimal bending of DNA upon complex formation (A. Manna and D.B., unpublished data). A model of the protein–DNA complex was constructed using these distance constraints in a computational simulation of a minimum energy structure. Although the model computed in this manner did not give precise information about bond angles and side-chain to base contacts, it did provide a biologically useful picture of how the two dimers were oriented on the DNA and thus provides material for future experiments.

The model of the RTP–DNA complex shown in Fig. 7, fitted the distance constraints derived from the EPD affinity cleavage data and the previously known information about the complex. In each of the core and auxiliary subsites of the IR1 terminus, both α3-helices inserted into the major groove and the antiparallel β2- and β3-strands had straddled the sugar phosphate backbone and occasionally inserted into the minor groove of the DNA. The major grooves had been forced open by the α3-helices necessitating a compensatory shrinkage of the adjacent minor grooves. The distortion was most noticeable near the center of the RTP dimer positioned on the core site and also at the region of apposition of the β2- to β3-strands. The core site was more distorted than the auxiliary site because the protein contacted the former site more often than the latter. The DNA was very slightly bent. However, we did not attempt to determine the degree of the bending. The two dimers are known to interact at the adjacent β3-strands of the two RTP dimers at the region of overlap between the core and the auxiliary sites (ref. 9 and Figs. 4 and 7). To accommodate this interaction, the dimers were brought together by a relative rotation of approximately 45° around the DNA. Appropriate constraints were introduced to maintain this interaction and the computer simulation was again performed. The DNA gets slightly unwound as a result of the β3–β3 interaction at the contact point between the two dimers. The model is consistent with all of the principal predictions made from the published crystallographic and genetic analyses (9, 14, 15) and, thus, provides a possible structural basis of the functional asymmetry of the replication terminus.

## DISCUSSION

Two alternative models have been considered in attempts to explain the mechanism of polar arrest of the replicative helicases and replication fork at the replication terminus. One model suggests the formation of a DNA–protein structure consisting of RTP and the terminus sequence that some how causes polar fork arrest without invoking protein–protein interaction between the terminator protein and the helicase. The second model postulates that both RTP–DNA interaction and specific interaction of a contrahelicase surface of RTP with a region of the helicase are necessary to effect polar fork arrest (24). To begin to derive evidence for one or the other of these mutually exclusive models, it was necessary to determine the structure of the terminus–terminator protein complex. The structure is expected to be useful in at least two ways. (*i*) It should yield information on how the two dimers of RTP are situated at the terminus and thus might provide clues as to the surface of RTP that is likely to make contact with the helicase. (*ii*) It should provide clues as to how structural and functional asymmetry of the DNA–protein complex is generated in spite of the structural symmetry of the apoprotein dimers.

Since the functional unit of the terminus contains four turns of DNA and two interacting dimers of RTP, a structure that is probably too large and flexible to be suitable for structure determination by x-ray crystallography, we resorted to the EPD-conjugation and affinity-cleavage procedure to derive at least an overall picture of the protein–DNA complex. Two assumptions implicit in this approach are that the most fre-

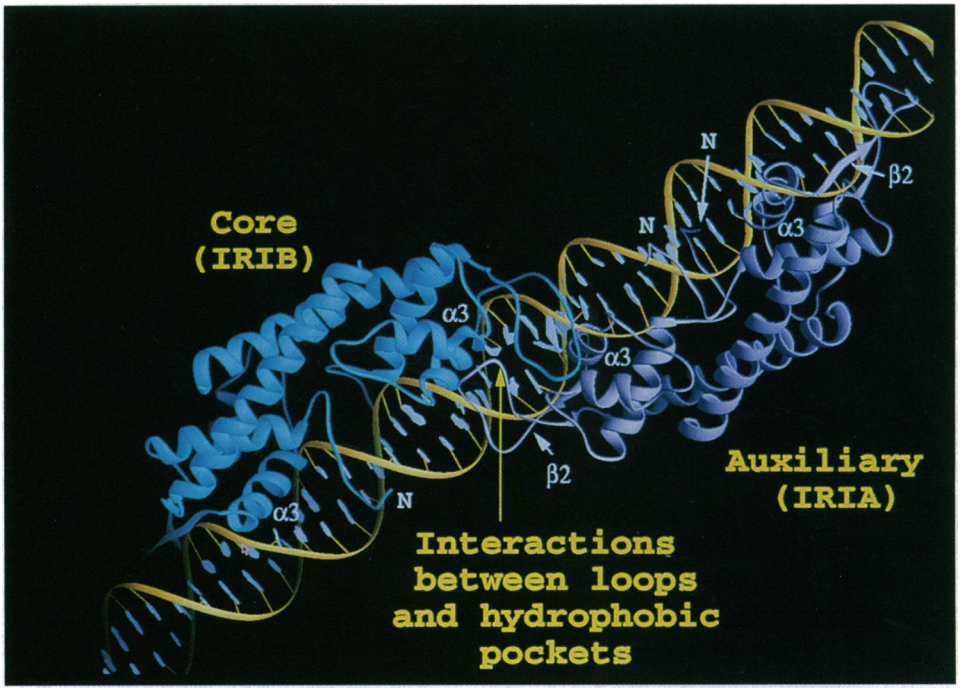


FIG. 7. Model of the three-dimensional structure of the IR1–RTP complex generated from affinity cleavage and the published crystallographic and genetic analyses. The Leu residue at the tip of the extended loop of monomer, as indicated by the arrow, interacts with the hydrophobic pocket of the adjacent monomer unit belonging to the second RTP dimer. The DNA is partially unwound at the dimer–dimer interaction region and has a slight curvature that is difficult to see in the illustration. The N-terminal (N) arms are poised over the sugar phosphate backbone. The α3-helices and the β3-strands are shown. Note that the major grooves have been extended at the regions of insertion of the α3-helices with a corresponding contraction of the minor grooves.

quent cleavage sites (the strongest cleavage products as seen in the autoradiograms) are located closest to the hydroxyradical generator, i.e., the Fe atom (Fig. 2*B*), and that the conjugation of EPD to RTP did not qualitatively alter the normal pattern of protein–DNA interaction although, as expected, the strength of DNA binding was reduced by EPD conjugation at certain residues.

From a comparative study of Fe-EDTA-induced affinity cleavage patterns of CAP protein–DNA complex, with the amino acid side chain to base contact as revealed by site-directed azido crosslinkage and from the known crystal structure of CAP–DNA complex, Chen and Ebright (25) observed close agreement on contacts as measured by all three procedures. Thus, affinity cleavage appears to be a reliable indicator of side chain to base contacts. We have also performed site-directed crosslinking studies between derivatized RTPs and the terminus DNA but have observed that unlike CAP and LexA (25, 26), RTP-DNA crosslinks were not sensitive to cleavage by alkali and thus could not be mapped by the alkali cleavage procedure (17).

The crystal structure revealed that the protein contains an unstructured N-terminal arm, a coiled-coil antiparallel dimerization domain involving the $\alpha$4-helix of each monomer (14). From stereochemical considerations, it was suggested that the two $\alpha$3-helices might recognize specific nucleotide sequences in the major groove of the DNA, the $\beta$2- and $\beta$3-strands, and the extended loop connecting the two might contact the minor groove (14). Mutational analyses of RTP in conjunction with site-directed protein–DNA crosslinking studies showed that the N-terminal arm, the $\beta$2-strand and the $\alpha$3-helix formed the DNA binding elements (15). Although the interaction of RTP with the terminus has been studied by various footprinting methods (6, 13, 23), more precise information on specific amino acid to base contacts were not available. The model presented in this paper is consistent with the following predictions made from a consideration of the crystal structure. The model confirms that the $\alpha$3-helix makes contacts with the major groove of the DNA and that the $\beta$2-strand, that is part of the wing, makes contact with the minor groove. The observation that the residues R16 of the $\alpha$1-helix and E63 of the $\alpha$3-helix contact the same residues at the middle of the core and auxiliary sites is understandable considering the fact that Arg-16 and Glu-63 are only separated by 9 Å.

The origin of structural asymmetry that most probably underlies the functional polarity is also illuminated by the model. For example, the derivative R59C contacts the core site at many more locations than at the auxiliary site whereas E56C seems to contact only the core and not the auxiliary site, thus contributing to generation of asymmetry.

The model positions the region of the amino acid residues 30–33 (the region between $\alpha$1 and $\beta$1 and including $\beta$1; Fig. 1) that projects outward from the surface of RTP in such a way that these could conceivably contact an approaching DnaB helicase that unwinds DNA ahead of the replication fork. RTP is also known to impede RNA polymerases in a polar mode (27). Our recent results suggest that mutational alteration in the region of amino acids 30–33 (connector between $\alpha$1 and $\beta$1 and extending through $\beta$1; Fig. 1) abolishes contrahelicase and RNA polymerase arresting activities of RTP without detectable alteration of DNA binding, dimerization, and dimer–dimer interaction activities, thus confirming the location of the contrahelicase surface (A. Manna, K.S.P., D.E.B., C. Davies, S.W.W. and D.B., unpublished results).

We thank Drs. Richard Ebright and David Sigman for many useful discussions. We are most grateful to Drs. Robert Fox and Venki Ramakrishnan for generous gifts of EPD. This work was supported by Grant GM49264 awarded to D.B. and S.W.W. and by Merit Award R37 AI19881 to D.B.

1. Yoshikawa, H. & Sueoka, N. (1963) *Proc. Natl. Acad. Sci. USA* **49,** 559–556.
2. Yoshikawa, H. & Sueoka, N. (1963) *Proc. Natl. Acad. Sci. USA* **49,** 806–813.
3. Franks, A. H., Griffith, A. A. & Wake, R. G. (1995) *Mol. Microbiol.* **17,** 13–23.
4. Smith, M. T. & Wake, R. G. (1992) *J. Mol. Biol.* **227,** 648–657.
5. Kaul, S., Mohanty, B. K., Sahoo, T., Patel, I., Khan, S. A. & Bastia, D. (1994) *Proc. Natl. Acad. Sci. USA* **91,** 1113–11147.
6. Sahoo, T., Mohanty, B. K., Patel, I. & Bastia, D. (1995) *EMBO J.* **14,** 619–648.
7. Lewis, P. J., Ralston, G. B., Christopherson, R. I. & Wake, R. G. (1989) *J. Mol. Biol.* **214,** 73–84.
8. Smith, M. T., Langley, D. B., Young, P. A. & Wake, R. G. (1994) *J. Mol. Biol.* **241,** 335–340.
9. Manna, A. C., Pai, K. S., Bussiere, D. E., White, S. W. & Bastia, D. (1996) *Proc. Natl. Acad. Sci. USA* **93,** 3253–3258.
10. Young, P. A. & Wake, R. G. (1994) *J. Mol. Biol.* **240,** 275–280.
11. Sahoo, T., Mohanty, B. K., Lobert, M., Manna, A. C. & Bastia, D. (1995) *J. Biol. Chem.* **270,** 29138–29144.
12. Lewis, P. J., Smith, M. T. & Wake, R. G. (1989) *J. Bacteriol.* **171,** 3564–3567.
13. Carrigan, C. M., Peck, R. A., Smith, M. T. & Wake, R. G. (1991) *J. Mol. Biol.* **222,** 197–207.
14. Bussiere, D. E., Bastia, D. & White, S. W. (1995) *Cell* **80,** 651–660.
15. Pai, K. S., Bussiere, D. E., Wang, F., Hutchison, C. A., White, S. W. & Bastia, D. (1996) *EMBO J.* **15,** 3164–3173.
16. Ermacora, M. R., Delfino, J. M., Cuenoud, B., Schepartz, A. & Fox, R. O. (1992) *Proc. Natl. Acad. Sci. USA* **89,** 6383–6387.
17. Ebright, Y. W., Chen, Y., Pendergrast, P. S. & Ebright, R. H. (1992) *Biochemistry* **31,** 10664–10670.
18. Mazzarelli, J. M., Ermacora, M. R., Fox, R. O. & Grindley, N. D. F. (1993) *Biochemistry* **32,** 2979–2986.
19. Pan, C. Q., Landgraf, R. & Sigman, D. (1994) *Mol. Microbiol.* **12,** 335–342.
20. Kunkel, T., Bebeneck, K. & McClary, J. (1991) *Methods Enzymol.* **204,** 125–138.
21. Oakley, M. G. & Dervan, P. B. (1990) *Science* **248,** 847–850.
22. Brunger, A. T. (1988) X-PLOR: A System for X-Ray Crystallography and NMR (Yale Univ. Press, New Haven, CT).
23. Langley, D. B., Smith, M. T., Lewis, P. J. & Wake, R. G. (1993) *Mol. Microbiol.* **10,** 771–779.
24. Khatri, G. S., MacAllister, T., Sista, P. R. & Bastia, D. (1989) *Cell* **59,** 667–674.
25. Chen, Y. & Ebright, R. H. (1993) *J. Mol. Biol.* **230,** 453–460.
26. Dumoulin, P., Oertel-Buchheit, P., Granger-Schnarr, M. & Schnarr, M. (1993) *Proc. Natl. Acad. Sci. USA* **90,** 2030–2034.
27. Mohanty, B. K., Sahoo, T. & Bastia, D. (1996) *EMBO J.* **15,** 2530–2539.